Wavelength dependent isotope fractionation in visible light O_3 photolysis and atmospheric implications

Marion Früchtl[1], Christof Janssen[2, 3], Domenico Taraborrelli[4], Sergey Gromov[4,5] and Thomas Röckmann[1]

Accepted Article

[1]Institute for Marine and Atmospheric Research Utrecht (IMAU), Utrecht University, 3584 CC Utrecht, The Netherlands.

[2]LERMA, Observatoire de Paris, PSL Research University, CNRS, UMR 8112, F-75014, Paris, France

[3]Sorbonne Universités, UPMC Univ Paris 6, UMR 8112, LERMA, F-75005 Paris, France

[4]Max Planck Institute for Chemistry, Hahn-Meitner Weg 1, D-55128 Mainz, Germany

[5]Institute of Global Climate and Ecology (IGCE Roshydromet and RAS), Glebovskaya 20b, 107258 Moscow, Russia

This article has been accepted for publication and undergone full peer review but has not been through the copyediting, typesetting, pagination and proofreading process which may lead to differences between this version and the Version of Record. Please cite this article as doi: 10.1002/2015GL066219

©2015 American Geophysical Union. All rights reserved.

Corresponding author: M. Früchtl, Institute for Marine and Atmospheric Research Utrecht (IMAU), Utrecht University, Princetonplein 5, 3584 CC Utrecht, The Netherlands. (m.fruechtl@uu.nl)

Accepted Article

©2015 American Geophysical Union. All rights reserved.

Key Points

- Visible light photolysis of O_3 leads to isotope enrichment of the remaining O_3
- Fractionation in visible light photolysis of O_3 is wavelength dependent
- The wavelength dependence is weaker than predicted by theory

Accepted Article

Abstract

The ^{17}O and ^{18}O isotope fractionation associated with photolysis of O_3 in the Chappuis band was determined using a broadband light source with cutoff filters at 455, 550, 620nm and narrow band light sources at 530, 617 and 660nm. The isotope effects follow a mass-dependent fractionation pattern ($\delta^{17}O/\delta^{18}O = 0.53$). Contrary to theoretical predictions, fractionations are negative for all wavelength ranges investigated and do not change sign at the absorption cross-section maximum. Our measurements differ from theoretical calculations by as much as 34 ‰ in $^{18}\varepsilon_{O_3+h\nu}$ = ($^{18}J/^{16}J-1$). The wavelength dependence is also weaker than predicted. Photo-induced fractionation is strongest when using a low wavelength cut-off at 620nm with $^{18}\varepsilon_{O_3+h\nu}$ = −26.9(±1.4)‰. With decreasing wavelength, fractionation values diminish to $^{18}\varepsilon_{O_3+h\nu}$= −12.9(±1.3)‰ at 530nm. Results from an atmospheric model demonstrate that visible light photolysis is the most important tropospheric sink of O_3, which thus contributes about 1/6 to the ozone enrichment.

©2015 American Geophysical Union. All rights reserved.

1. Introduction

Ozone (O_3) carries a strong enrichment (~ 100‰) in both heavy oxygen isotopes ^{17}O and ^{18}O compared to atmospheric O_2 [*Mauersberger*, 1981; *Krankowsky et al.*, 1995, 2007; *Johnson et al.*, 2000]. This enrichment shows a marked deviation from classical mass dependent fractionation, where $\delta^{17}O \approx 0.52 \times \delta^{18}O$. Mass-independent isotope fractionation can be quantified by the ^{17}O excess

$$\Delta^{17}O = \delta^{17}O - 0.52 \times \delta^{18}O. \quad (1)$$

The peculiar high enrichments in the heavy isotopes ^{17}O and ^{18}O originate from the O_3 formation reaction [*Krankowsky et al.*, 1995; *Johnson et al.*, 2000; *Mauersberger et al.*, 2001] and strongly depend on temperature and pressure [*Morton et al.*, 1990; *Thiemens and Jackson*, 1990; *Krankowsky et al.*, 2007]. In addition, atmospheric studies suggested a contribution of processes other than O_3 formation to the observed isotope enrichments in atmospheric O_3. At altitudes above 30 km atmospheric fractionations were between 35 and 40‰ higher than what is expected from the known isotope effects in O_3 formation [*Haverd et al.* 2005, *Krankowsky et al.* 2007]. The observed additional enrichment was tentatively attributed to the process of O_3 photolysis.

A semi-analytical theory to calculate photolysis induced isotope effects in O_3 and other gases [*Miller and Yung*, 2000; *Miller et al.* 2005; *Liang et al.* 2006] predicts pronounced wavelength-dependent isotope effects during photolysis. In the Chappuis band (400-800 nm) calculated fractionations show significantly nanometer-scale

©2015 American Geophysical Union. All rights reserved.

Accepted Article

variability superimposed on a general trend from positive fractionation on the short-wavelength side of the absorption maximum to strongly negative fractionation at the long-wavelength tail [*Liang et al.*, 2006]. *Ndengué et al.* [2010, 2012, 2014] performed improved calculations of isotope specific absorption cross-sections, using quantum mechanical MCTDH (Multiconfiguration Time-Dependent Hartree) wave packet propagation on ab-initio surfaces, but the cross sections are not provided which impedes direct comparison. For both types of calculation, model results show that the photolysis induced isotope effects contribute significantly to the isotopic composition of O_3 in the atmosphere [*Liang et al.* 2006, *Ndengué et al.* 2014]. While *Ndengué et al.* [2014] claim a strict mass dependence for O_3 photo-dissociation, the results of their atmospheric calculations show a ^{17}O excess of 2.5 to 3.5‰ at altitudes up to 32 km. If these numbers are significant, they will imply a non mass-dependent isotope fractionation from photolysis in the Huggins and/or Chappuis bands.

Due to the inherent approximations in the theoretical treatments, experimental studies are required to provide benchmark data. *Morton et al.* [1990] reported no significant change in O_3 when photolyzed with visible light, whereas *Chakraborty and Bhattacharya* [2003] found a mass dependent fractionation pattern ($\delta^{17}O/\delta^{18}O = 0.54$) for photolysis of O_3 at 520 nm and 630 nm. The fractionation coefficients they obtained for both wavelengths showed similar values of ${}^{18}\varepsilon_{O_3+h\nu}$ = −13.7±2‰ and ${}^{17}\varepsilon_{O_3+h\nu} = -7.25\pm0.1$. However, the calculations by *Liang et al.* [2006] yielded very different fractionations for photolysis at the two wavelengths, ${}^{18}\varepsilon_{O_3+h\nu}$= +5.8‰ at 520 and ${}^{18}\varepsilon_{O_3+h\nu} = -31$‰ at 630nm (average values for the symmetric and

©2015 American Geophysical Union. All rights reserved.

Accepted Article

asymmetric isotopomers).

A complication of the above photolysis experiments using pure O_3 samples is that the O atom that is produced during photolysis generally destroys another O_3 molecule in the reaction $O + O_3$. Thus, isotope effects in photolysis and chemical removal cannot be disentangled [*Brenninkmeijer et al.* 2003]. *Früchtl et al.* [2015] combined photolysis experiments of pure O_3 and O_3 mixed in a large excess of CO, which acts as O atom quencher, to separately quantify the fractionation in both removal processes. Photolysis experiments using a broadband light source with a 455 nm long-pass filter yielded ${}^{18}\varepsilon_{O_3+h\nu} = -16.1(\pm1.4)‰$ and ${}^{17}\varepsilon_{O_3+h\nu} = -8.05(\pm0.7)‰$, and ${}^{18}\varepsilon_{O_3+O} = -11.9(\pm1.4)‰$ and ${}^{17}\varepsilon_{O_3+O} = -5.95(\pm0.7)‰$. Notably, both fractionations are mass dependent.

Following up on these results, we examine here the (low resolution) wavelength dependence of the isotope fractionation in the photolysis of O_3 by visible light using various light sources and cut-off filters.

2. Methods

2.1 Experimental procedure

The experimental system has been described in detail in *Früchtl et al.* [2015]. O_3 was produced by electric discharge from ~8.0 hPa of pure O_2 (99.9998%) in a spherical 1.0 L glass reactor with a cylindrical extension immersed in liquid nitrogen (LN_2). O_3 condensed at the reactor wall and the remaining O_2 was pumped away. Subsequently

©2015 American Geophysical Union. All rights reserved.

Accepted Article

O_3 was brought to room temperature, and an aliquot was expanded to the cylindrical photolysis chamber (V = 630 cm^3) for photolysis. After photolysis, the leftover O_3 was separated from O_2 by pumping the mixture through a cryogenic trap cooled to the triple point temperature of N_2 (63K). At this temperature O_3 condenses but O_2 produced during photolysis does not and can be pumped away. The collected O_3 was transferred to a sample bottle (V=44 cm^3) containing molecular sieve (13X) immersed in LN_2 and subsequently converted to molecular O_2 by heating. The amount of O_2 originating from O_3 was then determined by measuring the pressure after transfer to a reference volume (V=1.8 cm^3, containing molecular sieve). The isotopic composition was determined on a Dual Inlet IRMS (Thermo Finnigan Delta Plus XL) with an uncertainty of 0.03‰ for $\delta^{18}O$ and 0.08‰ for $\delta^{17}O$ (n = 150).

Two sets of photolysis experiments were conducted. In a first set, a broadband light source (λ = 400 to 800 nm) with an emission peak at 605 nm was used (tungsten halogen lamp, Osram HLX 64633, described in *Früchtl et al.* [2015]). To select different wavelength regions, we used different optical long pass glass color filters with cutoff wavelengths at 455±6, 550±6 or 620±5 nm (GG455, OG550, Schott; R-620, Hoya). For each experiment the corresponding filter was placed between the lamp and the photolytic chamber. In a second set, three narrow band light sources (high power LEDs) with emission peaks at 530, 617 and 660 nm and respective bandwidths (FWHM) of 33, 18 and 25 nm were used (Thorlabs M530L3, M617L3 and M660L3).

Each experiment consisted of measuring three aliquots from the same initial O_3 reservoir. The first aliquot expanded into the photolysis chamber was used as

©2015 American Geophysical Union. All rights reserved.

Accepted Article

control measurement to correct for small O_3 losses that occur without photolysis. The second aliquot (expansion #2) was collected after 10 to 30 minutes of photolysis. The final aliquot (expansion #3) is the residual O_3 in the discharge reactor, which represents the original O_3 produced in the electric discharge.

In the following we refer to the amount of the photolyzed sample (expansion #2, corrected for the control experiment) as $O_3(end)$ and the remaining O_3 from the discharge reactor (expansion #3) as $O_3(start)$. The remaining fraction $f(O_3)$ after a certain time t of photolysis is defined as $f(O_3) = O_3(end)/O_3(start)$. Isotope enrichments are reported as $\delta^x O = (N(^xO)/N(^{16}O))_{SA}/(N(^xO)/N(^{16}O))_{ST} - 1$, where x indicates heavy isotope mass numbers 18 or 17. δ quantifies the relative deviation of the ratio $N(^xO)/N(^{16}O)$ of isotope abundances (N) in a sample (SA) from the same ratio in a standard material (ST). Values are reported in per mill (‰). The isotopic composition of initial O_3 is chosen as standard.

2.2. Photolysis rate and fractionations in O_3 photolysis

The photolysis rate J is determined from the temporal evolution of O_3 removal (f) in the experiments

$$J = 0.5\ln(f)/t. \quad (3)$$

Measured photolysis rates range from $3.3(\pm0.06)\times10^{-4}$ s^{-1} (455 nm filter) to $0.9(\pm0.3)\times10^{-4}$ s^{-1} (530 nm LED) (Table 1). The spectral photolysis rate for each light source is shown in Figure 2a. Values are calculated by multiplying O_3 absorption

©2015 American Geophysical Union. All rights reserved.

Accepted Article

cross sections [*Sander et al.*, 2011] with the spectral actinic flux under the assumption of unit quantum yield. The spectral actinic flux with different filters was obtained by multiplication of the actinic flux of the halogen lamp without filter (determined with a spectral photometer, model 752, Optronic laboratories Inc., USA) with the filter internal transmittance published by the manufacturer. For LED light sources, the spectral actinic flux data provided by the manufacturer were used.

2.3. Control measurements and error estimates

The stability of the analytical system was characterized by *control* measurements without irradiation as described above. A loss of 4-7% of O_3 was observed in the control experiments, associated with changes of $\delta^{18}O < 0.1‰$ and $\delta^{17}O < 0.05‰$. For correction, average values from the control measurements were subtracted from the raw data of the photolysis experiments.

Uncertainty estimates for $\delta^{18}O$ and $\delta^{17}O$ include errors from control measurements $(\sigma_{control})$ and IRMS measurements ($\sigma_{O_3 end}$, $\sigma_{O_3 start}$) according to

$$\sigma = \sqrt{(\sigma_{O_3 end})^2 + (\sigma_{O_3 start})^2 + (\sigma_{control})^2}, \quad (2)$$

total errors are <0.2 ‰ for ^{17}O and ^{18}O.

Uncertainties in ln(*f*) as a consequence of the applied sampling procedure were derived from experiments with pure CO_2 instead of O_3, because CO_2 is easy to trap and transfer in vacuum systems with virtually no loss (>99.5% recovery). Considering a small non-linearity of the pressure sensor, errors in pressure reading and small

©2015 American Geophysical Union. All rights reserved.

Accepted Article

changes in temperature, total relative uncertainties in ln(*f*) are between 2.6 and 2.8% [*Früchtl et al.*, 2015].

3. Results

Figure 1a-d shows that, independent of the light source used, the remaining O_3 becomes isotopically enriched during the photolysis experiments, i.e., the heavy isotopologues are removed more slowly than $^{16}O_3$ for all wavelength ranges. The measured fractionations ε for ^{18}O vary between −12.4‰ and −19.4‰ and between −6.7‰ and −10.2‰ for ^{17}O (Figure 1b,d and Table 1). O_3 photolysis with the broadband lamp using a 550 nm or a 455 nm filter or the 617 nm LED, result in very similar fractionations (Table 1). For these experiments the peak emission is slightly above 600 nm. The fractionations become more negative towards longer wavelength (620 nm filter, 660 nm LED). At shorter wavelength (530 nm), the fractionations values are highest, but still clearly negative at $^{18}\varepsilon = -12.4$‰ and $^{17}\varepsilon = -6.7$‰.

As mentioned above, the observed fractionation in the photolysis experiments with pure O_3 does not only include O_3 photolysis (R1) but due to the photolytic production of O atoms, also the chemical O_3 removal via R2.

(R1) $O_3 + h\nu \rightarrow O_2 + O$

(R2) $O + O_3 \rightarrow 2O_2$

(R3) $O + O_2 + M \rightarrow O_3 + M$

In our experiments the rates of O_3 photolysis (R1) and O_3 + O (R2) are very similar and reformation of O_3 via (R3) is negligible (<1%). These conclusions are in line with isotope kinetic modeling (not shown). Thus, the total fractionation (ε_{total}) is the

©2015 American Geophysical Union. All rights reserved.

Accepted Article

average of the two fractionations in reactions R1 and R2

$$\varepsilon_{total} = (\varepsilon_{O_3+h\nu} + \varepsilon_{O_3+O})/2. \quad (4)$$

Using the previously determined fractionation values for (R2) of ${}^{18}\varepsilon_{O_3+O}$ = −11.9(±1.4)‰ and ${}^{17}\varepsilon_{O_3+O}$ = −5.95(±0.7)‰ [*Früchtl et al.*, 2015], the photolysis induced fractionations can be calculated from equation (4).

The resulting fractionations attributed to O_3 photolysis are shown in Table 1 and Figure 2b,c. For all the wavelength intervals investigated, photolysis of O_3 induces negative fractionations, with a trend to stronger isotopic fractionation at longer wavelengths. Measured fractionations range between −26.9‰ and −12.9‰ for ^{18}O and −14.4‰ and −7.5‰ for ^{17}O in experiments applying a 620nm filter or the 530nm LED respectively. Figure 2 also shows the wavelength dependent fractionations calculated by *Liang et al.* [2004, 2006]. By convolving these fractionations with the photolysis spectra of our light sources the predicted photo induced fractionations for our experimental conditions were calculated (Table 1, Figure 2b,c).

The theoretical predictions agree best with the experiments using the broadband lamp with 550 nm filter or 660 nm LED, with maximum differences of only 3.3‰ for ${}^{18}\varepsilon_{O_3+h\nu}$ and 1.8‰ for ${}^{17}\varepsilon_{O_3+h\nu}$. In qualitative agreement with calculations [*Liang et al.*, 2006] we observe a wavelength dependence and stronger fractionations at longer wavelengths. At shorter wavelengths, however, the observed

©2015 American Geophysical Union. All rights reserved.

Accepted Article

wavelength dependence is much smaller than predicted and discrepancies become considerable (33.9‰ and 18.5‰ for $^{18}\varepsilon_{O_3+h\nu}$ and $^{17}\varepsilon_{O_3+h\nu}$ at 530 nm). Most importantly, the experimentally determined fractionations do not show change in sign towards shorter wavelengths, whereas the calculations predict a change from negative to positive values below 600 nm.

Figure 3 shows the three-isotope plot ($\delta^{17}O/\delta^{18}O$) for all photolysis experiments. There is no significant difference between the three-isotope slopes of individual experiments and a fit to all data follows a slope of 0.534 (±0.003) at a confidence level of 99%, which is in agreement with previous results from *Chakraborty and Bhattacharya* [2003].

4. Discussion

A possible systematic uncertainty in the experimental determination of the photolysis-induced fractionation is due to the need to correct for the fractionation in the O + O_3 reaction. The correction depends on the results of *Früchtl et al.* [2015], where unexplained losses of O_3 might have introduced systematic errors in the determination of ε_{O_3+O}. Estimating the effects of these errors yielded lower limits of $^{18}\varepsilon_{O_3+O}$ = −18.6‰ and $^{17}\varepsilon_{O_3+O}$= −9.3‰ [*Früchtl et al.*, 2015]. According to Eq. 4, lower values assigned to ε_{O_3+O} would lead to correspondingly higher values for $\varepsilon_{O_3+h\nu}$. However even for the estimated lower limits for ε_{O_3+O}, the photolysis induced fractionations $\varepsilon_{O_3+h\nu}$ would remain negative over all of the wavelength ranges investigated with highest values of $^{18}\varepsilon_{O_3+h\nu}$ =−6.2‰ and $^{17}\varepsilon_{O_3+h\nu}$ =−4.2‰. Therefore

©2015 American Geophysical Union. All rights reserved.

Accepted Article

the strong discrepancy between our measurements and the theoretical calculations by *Liang et al.* [2006], which predict positive fractionations for $\lambda < 600$ nm, cannot be attributed to erroneous assumptions in ε_{O_3+O}.

Isotope effects in O_3 photolysis result from variations of the transition dipole moment (TDM) with isotopic substitution [*Schinke*, 1993]. Since the semi-empirical zero-point energy approach is based on the main isotopologue only, variations in TDM with isotopic substitution cannot be predicted accurately. For photolysis of N_2O, results from ab-initio calculations agree better with experimentally determined isotope fractionations than semi-empirical calculations [*Schmidt et al.,* 2011]. For CO_2, the ab-initio calculations [*Schmidt et al.,* 2013] reported three times stronger fractionations than predicted by the semi-empirical approach applied by *Liang et al.* [2004]. Furthermore, *Ndengué et al.* [2014] showed that the assumption by *Liang et al.* [2004] of a proportional relationship between changes in absorption cross sections under isotopic substitution and changes in zero point energy for both central and terminal substitution is not valid. This suggests that the discrepancies in magnitude and wavelength dependence between our observations and the theoretical calculations by *Liang et al.* [2004, 2006] are likely to arise from shortcomings in the semi-analytical approach. The observed weak wavelength dependency of ε is experimentally supported by the results of *Chakraborty and Bhattacharya* [2003] who found similar fractionations for O_3 photolysis at 520(±2) and 630(±4) nm, although they could not take into account the $O_3 + O$ reaction.

In order to assess the implications of our results for O_3 photolysis in the

©2015 American Geophysical Union. All rights reserved.

Accepted Article

atmosphere, Figure 2a includes the spectral photolysis rate calculated using a typical solar actinic flux spectrum. This spectral photolysis rate is quite similar to that achieved with the broadband photolysis lamp using the 455 nm long pass filter, with the solar curve being slightly blue-shifted. The relatively weak wavelength dependence of the fractionation found in our experiments implicates that the overall fractionation under solar irradiation should be rather similar to the value obtained with the broadband lamp and the 455 nm filter. The blue-shift of the solar photolysis rate would result in a slightly larger contribution from the short-wave tail with lower fractionations and a smaller contribution from the long-wave tail with stronger fractionations. Since these tail regions are not well covered by our experiments, precise quantification is not possible at present but we estimate that the total fractionation in the atmosphere may be a few per mill lower than $^{18}\varepsilon_{O_3+h\nu}$ = −16.1 (±1.1)‰ and $^{17}\varepsilon_{O_3+h\nu}$ = −8.9(±0.6)‰ which was found with the broadband lamp and the 455 nm filter (Table 1, *455 nm filter*). Compared to a total fractionation of 90‰ observed for atmospheric O_3 [*Krankowsky et al.* 2007, *Johnston and Thiemens* 1997] the fractionation in visible light O_3 photolysis is of significant magnitude and needs to be considered when investigating isotope effects of ozone.

Ozone is a highly reactive molecule and its isotopic composition in the atmosphere is determined by the dynamic balance between isotope fractionation in ozone formation and in its gross loss. In order to quantify the importance of Chappuis band photolysis as gross removal process, we analyzed the turnover of O_3 in the global model EMAC (ECHAM5/MESSy

©2015 American Geophysical Union. All rights reserved.

Accepted Article

Atmospheric Chemistry, [*Jöckel et al.*, 2006, 2010]). EMAC is equipped with the comprehensive chemical mechanism accounting for all relevant gas-phase and photolytic O_3 reactions [*Taraborrelli et al.*, 2012], further revised and extended with monoterpenes/aromatics chemistry including ozonolysis [*Bloss et al.*, 2005; *Hens et al.*, 2014; *Nölscher et al.*, 2014; *Peeters et al.*, 2014]. The EMAC photolysis sub-model [*Sander et al.*, 2014] provides wavelength-resolved photolysis rates and their integrals for the channels leading to $O(^3P)$ and $O(^1D)$ production. Photolysis in the Huggins band produces $O(^3P)$ and yields about 90% $O(^1D)$ and 10% $O(^3P)$ for the lower stratosphere and below. We diagnose that visible light photolysis in the Chappuis band accounts for more than 85% of the overall O_3 gross removal rate simulated by EMAC, from the free troposphere up to 50 hPa (Fig. 4a). Only in the regions strongly affected by anthropogenic emissions the removal via non-photolytic sinks (predominantly in NO_x and HO_x chemistry) is of similar importance as Chappuis band photolysis near the surface (Fig. 4b). Above 800 hPa, however, the photolytic sink clearly dominates (Fig. 4b). We conclude that the fractionation in Chappuis band photolysis globally affects the isotopic composition of O_3 in the troposphere.

The derived three-isotope slope of 0.534(±0.003) is at the upper end of the range that is usually considered as mass-dependent fractionation and the value is higher than the one used in the defining equation of $\Delta^{17}O$ (eq. 1). For ${}^{18}\varepsilon_{O_3+h\nu}$ values of −15‰ in atmospheric Chappuis band photolysis and a difference of 0.014 from ${}^{17}\delta/{}^{18}\delta = 0.52$ in the three-isotope slope, the corresponding $\Delta^{17}O$ values would be 0.2

©2015 American Geophysical Union. All rights reserved.

Accepted Article

to 0.3‰ (eq. 1). This is two orders of magnitude lower than $\Delta^{17}O$ of atmospheric O_3, which ranges between 25 and 40‰ [*Vicars and Savarino,* 2014; *Brenninkmeijer et al.,* 2003; *Krankowsky et al.*, 2007, *Johnston and Thiemens* 1997]. Therefore, the contribution of visible light photolysis to the mass-independent isotope signature of atmospheric O_3 could be negligible.

Our results further indicate that previous experiments to determine the isotope fractionation in O_3 formation via photolytic recycling of O_3 in an O_2 bath gas using visible light [*Morton et al.*, 1990] may be biased by non-negligible isotope effects in O_3 photolysis.

Whereas the results from this study suggest shortcomings in the calculation of the overall wavelength dependence of photolysis induced O_3 fractionation in the Chappuis band, the wavelength resolution of the light sources employed is insufficient to examine smaller scale (few nm and sub-nm) variability that was also predicted by the calculations [*Miller et al.*, 2005; *Liang et al.*, 2006]. Laser light sources could help to investigate this further, but high power is required to realize sufficient removal of O_3 in laboratory experiments.

Accepted Article

©2015 American Geophysical Union. All rights reserved.

Acknowledgements

The authors gratefully acknowledge support from the Marie Curie Initial Training Network INTRAMIF (**In**itial **Tra**ining Network on **M**ass **I**ndependent **F**ractionation) as part of the European Community's Seventh Framework Program (FP7/2007-2013), Grant 237890. We thank Matthew S. Johnson for his comments on the discussion of the model-derived isotope effects in ozone photolysis. The data presented in this paper are available at http://www.projects.science.uu.nl/atmosphereclimate/Data.php.

Accepted Article

References

Bloss, C. et al. (2005), Development of a detailed chemical mechanism (MCMv3.1) for the atmospheric oxidation of aromatic hydrocarbons, *Atmos. Chem. Phys.*, *5*(3), 641–664, doi:10.5194/acp-5-641-2005.

Chakraborty, S., and S. K. Bhattacharya (2003), Oxygen isotopic anomaly in surface induced ozone dissociation, *Chem. Phys. Lett.*, *369*(5-6), 662–667, doi:10.1016/S0009-2614(03)00018-6.

Früchtl, M., C. Janssen, and T. Röckmann (2015), Experimental study on isotope fractionation effects in visible photolysis of O_3 and in the $O + O_3$ odd oxygen sink reaction, *J. Geophys. Res. Atmos.*, 1-19, doi:10.1002/2014JD022944.

Haverd, V., G. C. Toon, and D. W. T. Griffith (2005), Evidence for altitude-dependent photolysis-induced 18O isotopic fractionation in stratospheric ozone, *Geophys. Res. Lett.*, *32*(22), L22808, doi:10.1029/2005GL024049.

Hens, K. et al. (2014), Observation and modelling of HOx radicals in a boreal forest, *Atmos. Chem. Phys.*, *14*(16), 8723–8747, doi:10.5194/acp-14-8723-2014.

Jöckel, P. et al. (2006), The atmospheric chemistry general circulation model ECHAM5/MESSy1: consistent simulation of ozone from the surface to the mesosphere, *Atmos. Chem. Phys.*, *6*, 5067−5104, doi:10.5194/acp-6-5067-2006.

Jöckel, P., A. Kerkweg, A. Pozzer, R. Sander, H. Tost, H. Riede, A. Baumgaertner, S. Gromov, and B. Kern (2010), Development cycle 2 of the Modular Earth

©2015 American Geophysical Union. All rights reserved.

Submodel System (MESSy2), *Geosci. Model Dev.*, *3*(2), 717−752, doi:10.5194/gmd-3-717-2010.

Johnson, D. G., K. W. Jucks, W. A. Traub, and K. V. Chance (2000), Isotopic composition of stratospheric ozone, *J. Geophys. Res.*, *105*(D7), 9025, doi:10.1029/1999JD901167.

Krankowsky, D., F. Bartecki, G. G. Klees, K. Mauersberger, K. Schellenbach, and J. Stehr (1995), Measurement of heavy isotope enrichment in tropospheric ozone, *Geophys. Res. Lett.*, *22*(13), 1713−1716, doi:10.1029/95gl01436.

Krankowsky, D., P. Lämmerzahl, K. Mauersberger, C. Janssen, B. Tuzson, and T. Röckmann (2007), Stratospheric ozone isotope fractionations derived from collected samples, *J. Geophys. Res. Atmos.*, *112*(D8), D08301, doi:10.1029/2006jd007855.

Liang, M.-C., G. A. Blake, and Y. L. Yung (2004), A semianalytic model for photo-induced isotopic fractionation in simple molecules, *J. Geophys. Res.*, *109*(D10), D10308, doi:10.1029/2004JD004539.

Liang, M.-C., F. W. Irion, J. D. Weibel, C. E. Miller, G. A. Blake, and Y. L. Yung (2006), Isotopic composition of stratospheric ozone, *J. Geophys. Res. Atmos.*, *111*(D2), D02302, doi:10.1029/2005jd006342.

Mauersberger, K. (1981), Measurement of Heavy Ozone in the Stratosphere, *Geophys. Res. Lett.*, *8*(8), 935−937, doi:10.1029/Gl008i008p00935.

Mauersberger, K., P. Lämmerzahl, and D. Krankowsky (2001), Stratospheric ozone isotope enrichments-revisited, *Geophys. Res. Lett.*, *28*(16), 3155–3158, doi:10.1029/2001GL013439.

Miller, C. E., and Y. L. Yung (2000), Photo-induced isotope fractionation, *J. Geophys. Res.*, *105*(D23), 29.

Miller, C. E., R. M. Onorato, M.-C. Liang, and Y. L. Yung (2005), Extraordinary isotopic fractionation in ozone photolysis, *Geophys. Res. Lett.*, *32*(14), L1481(11–4), doi:10.1029/2005GL023160.

Morton, J., J. Barnes, B. Schueler, and K. Mauersberger (1990), Laboratory studies of heavy ozone, *J. Geophys. Res. Atmos.*, *95*(D1), 901−907, doi:10.1029/JD095iD01p00901.

Ndengué, S., S. Madronich, F. Gatti, H.-D. Meyer, O. Motapon, and R. Jost (2014), Ozone Photolysis: strong isotopologue/isotopomer selectivity in the stratosphere, *J. Geophys. Res. Atmos.*, *119*, 4286–4302, doi:10.1002/2013JD020033.

Accepted Article

©2015 American Geophysical Union. All rights reserved.

Ndengué, S. A., F. Gatti, R. Schinke, H.-D. Meyer, and R. Jost (2010), Absorption Cross Section of Ozone Isotopologues Calculated with the Multiconfiguration, *J. Phys. Chem., 114*, 9855–9863.

Ndengué, S. A., R. Schinke, F. Gatti, H. D. Meyer, and R. Jost (2012), Ozone photodissociation: Isotopic and electronic branching ratios for symmetric and asymmetric isotopologues, *J. Phys. Chem. A*, *116*(50), 12271–12279.

Nölscher, A. C., T. Butler, J. Auld, P. Veres, A. Muñoz, D. Taraborrelli, L. Vereecken, J. Lelieveld, and J. Williams (2014), Using total OH reactivity to assess isoprene photooxidation via measurement and model, *Atmos. Environ.*, *89*, 453–463, doi:10.1016/j.atmosenv.2014.02.024.

Peeters, J., J.-F. Müller, T. Stavrakou, and V. S. Nguyen (2014), Hydroxyl Radical Recycling in Isoprene Oxidation Driven by Hydrogen Bonding and Hydrogen Tunneling: The Upgraded LIM1 Mechanism, *J. Phys. Chem. A*, *118*(38), 8625–8643, doi:10.1021/jp5033146.

Sander, R., P. Jöckel, O. Kirner, A. T. Kunert, J. Landgraf, and A. Pozzer (2014), The photolysis module JVAL-14, compatible with the MESSy standard, and the JVal PreProcessor (JVPP), *Geosci. Model Dev.*, *7*(6), 2653–2662, doi:10.5194/gmd-7-2653-2014.

Sander, S. P., , J. Abbatt, J.R. Barker, J.B. Burkholder, R.R. Friedl, D.M. Golden, R.E. Huie, C.E. Kolb, M.J. Kurylo, G. K. Moortgat, V.L. Orkin, and P.H. Wine (2011), Chemical Kinetics and Photochemical Data for Use in Atmospheric Studies Evaluation Number 17 NASA Panel for Data Evaluation No. 17, JPL Publication 10–6, Jet Propulsion Laboratory, Pasadena, http://jpldataeval.jpl.nasa.gov.

Schinke, R. (1993), Photodisccoiation dynamics, Cambridge monographs on atmoic, molecular and chemical physics 1, Cambridge Univeristy Press, Cambridge, pp. 412.

Taraborrelli, D., M. G. Lawrence, J. N. Crowley, T. J. Dillon, S. Gromov, C. B. M. Grosz, L. Vereecken, and J. Lelieveld (2012), Hydroxyl radical buffered by isoprene oxidation over tropical forests, *Nat. Geosci.*, *5*(3), 190−193, doi:10.1038/ngeo1405.

Thiemens, M. H., and T. Jackson (1990), Pressure dependence for heavy isotope enhancement in ozone formation, *Geophys. Res. Lett.*, *17*(6), 717–719.

Accepted Article

©2015 American Geophysical Union. All rights reserved.

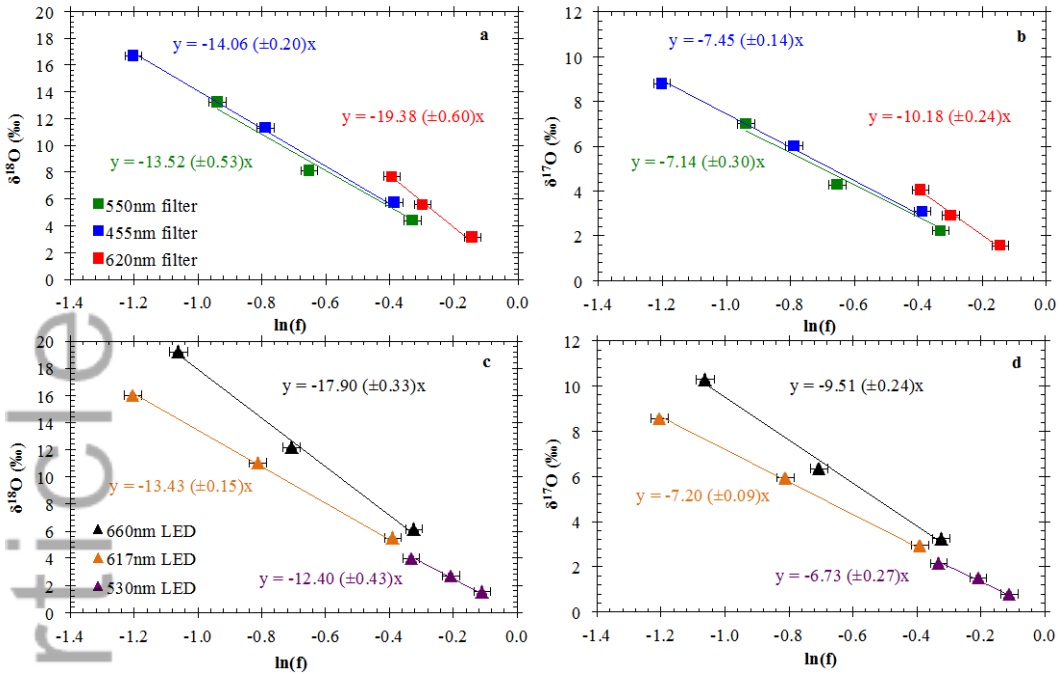

Figure 1 a-d: Rayleigh fractionation plots for O_3 photolysis experiments of 10, 20 and 30 minutes (three points in each series). Top: photolysis with the halogen lamp and different filters. Bottom: photolysis with high power LEDs. $\delta^{17}O$ and $\delta^{18}O$ are given versus O_3(*start*). Errors in the slopes (ε_{total}) are based on least square fits forced through zero. Errors in ln(f) are between 0.026 and 0.028. Errors in δ values are < 0.2‰.

Accepted Article

©2015 American Geophysical Union. All rights reserved.

Accepted Article

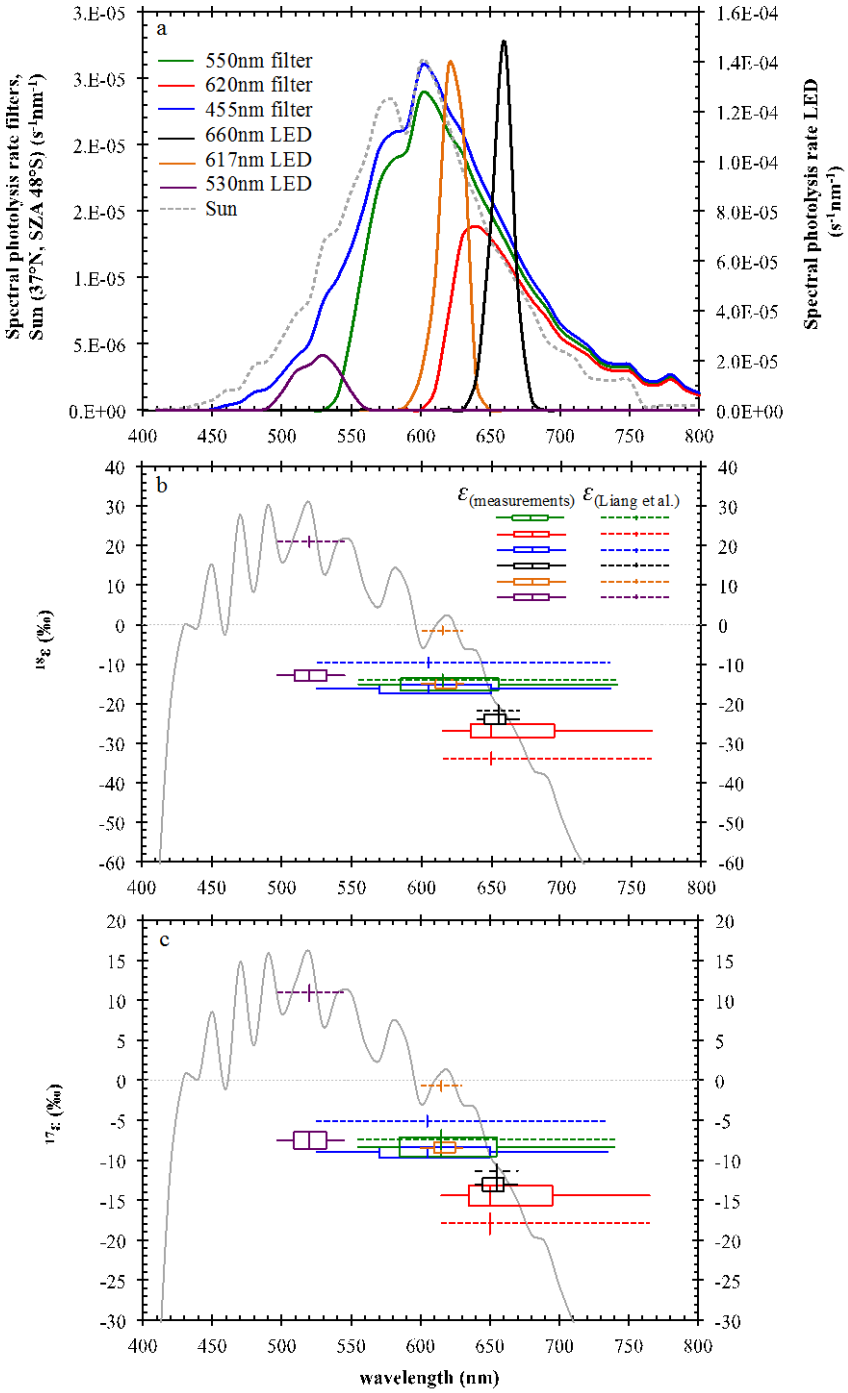

Figure 2: (a): Spectral photolysis rates for the different light sources used in the experiments. Green: 550nm filter, Red: 620nm filter, Blue: 455nm filter, Orange: 617nm LED, Black: 660nm LED, Purple: 530nm LED, Grey (dashed): Sun (37°N,

©2015 American Geophysical Union. All rights reserved.

SZA 48°S, from: http://rredc.nrel.gov/solar/spectra/am1.5/). Filter and LED data is scaled to the measured photolysis rate J of each light source (section 2.2) whereas the sun spectrum is scaled to $J_{455\text{nm filter}}$. b) and c): Isotope fractionations $^{18}\varepsilon$ and $^{17}\varepsilon$. Colours represent different filter and LEDs as defined in Figure 2a. The box width and solid horizontal lines indicate the wavelength intervals in which 50% and 90%, respectively, of the photons are emitted. Solid vertical lines indicate the medians. The height of the boxes marks the error for $\varepsilon_{O_3+h\nu}$ calculated as $\sigma_{O_3+h\nu} = \sqrt{(2\times\sigma_{\varepsilon(total)})^2 + (\sigma_{\varepsilon(O+O_3)})^2}$. The grey solid lines show the wavelength dependent fractionations as calculated by *Liang et al.* [2004, 2006]. The dashed lines show the fractionations expected from theoretical calculations by *Liang et al.* for our light sources.

Accepted Article

©2015 American Geophysical Union. All rights reserved.

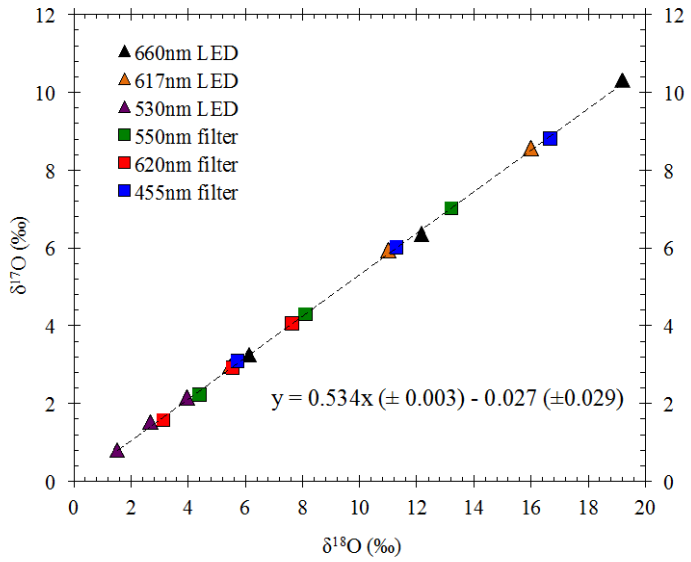

Figure 3: Three-isotope plot. Different symbols represent the different sets of experiments. The linear fit has a slope of 0.534±0.003 and a non-significant y-axis intercept.

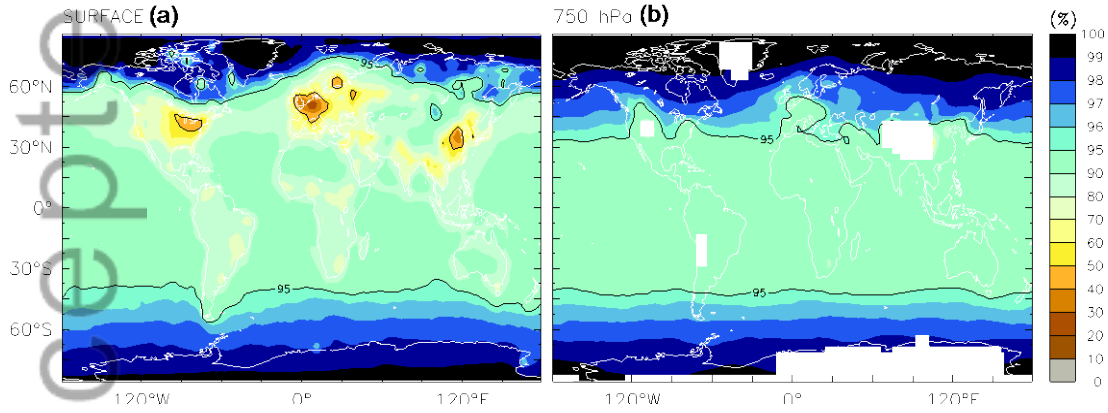

Figure 4: Fraction (in per cent) of the total O_3 sink attributed to photolysis leading to $O^3(P)$ production simulated by EMAC at the surface (a) and 750 hPa pressure (b) layers. Shown is a typical example from March 2001. White areas indicate regions

©2015 American Geophysical Union. All rights reserved.

Accepted Article

with surface pressures lower than 750 hPa; superimposed contours refer to 50% and 95% levels, respectively.

Table 1: Overview of measurement results compared to *Liang et al.* [2006].

	$J(s^{-1})$ ($\times 10^{-4}$)	$\varepsilon_{(total)}$ (‰)		$\varepsilon_{O_3+h\nu}$ (‰)		$\varepsilon_{(O_3+h\nu)\,Liang\,et.al}$ (‰)	
		^{18}O	^{17}O	^{18}O	^{17}O	^{18}O	^{17}O
455nm filter	3.34 (±0.06)	-14.1 (±0.2)	-7.5 (±0.1)	-16.2 (±1.1)	-8.9 (±0.6)	-9.6	-5.1
550nm filter	2.69 (±0.07)	-13.5 (±0.5)	-7.1 (±0.3)	-15.2 (±1.3)	-8.3 (±0.9)	-14.0	-7.4
620nm filter	1.18 (±0.08)	-19.4 (±0.6)	-10.2 (±0.2)	-26.9 (±1.4)	-14.4 (±1.0)	-34.0	-17.9
530nm LED	0.89 (±0.03)	-12.4 (±0.4)	-6.7 (±0.3)	-12.9 (±1.3)	-7.5 (±0.8)	20.9	10.9
617nm LED	3.33 (±0.07)	-13.4 (±0.2)	-7.2 (±0.1)	-15.0 (±1.1)	-8.4 (±0.6)	-1.5	-0.7
660nm LED	2.86 (±0.15)	-17.9 (±0.3)	-9.5 (±0.2)	-23.9 (±1.2)	-13.1 (±0.7)	-21.8	-11.4

Accepted Article

©2015 American Geophysical Union. All rights reserved.

Accepted Article

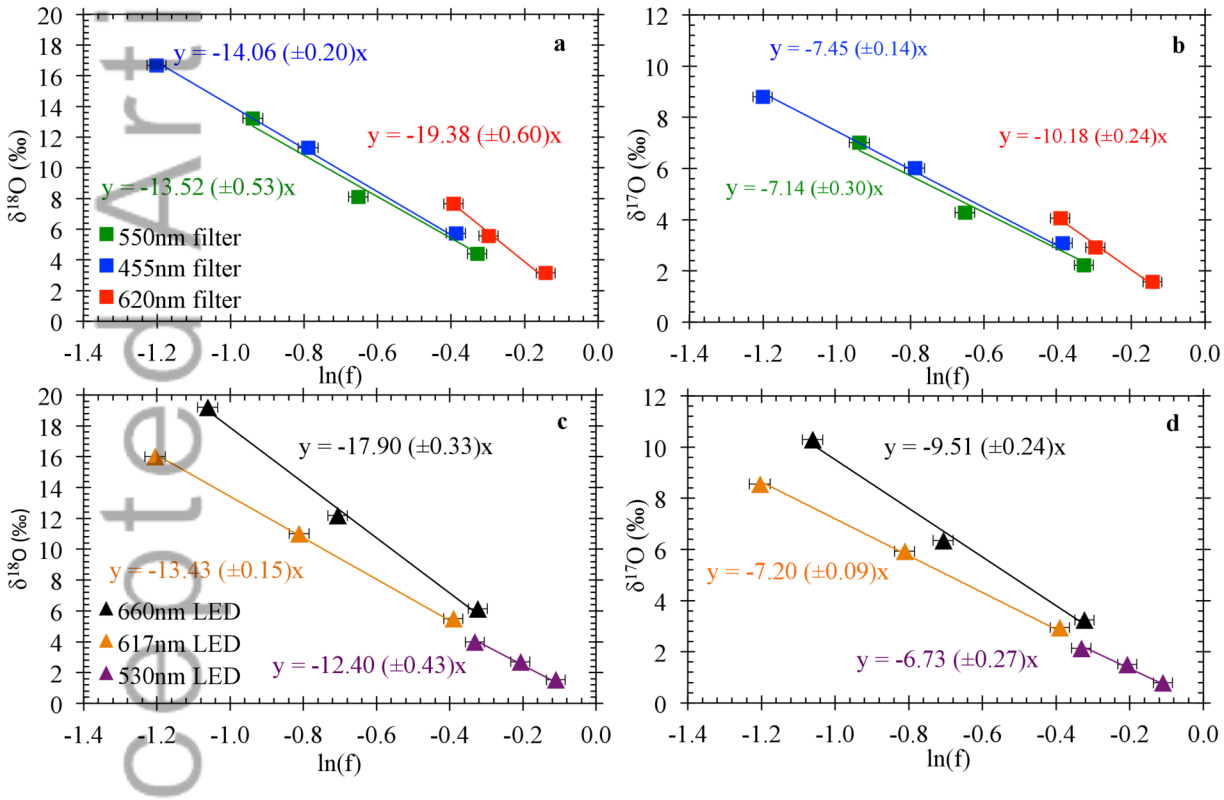

2015gl064192_figure01

©2015 American Geophysical Union. All rights reserved.

Accepted Article

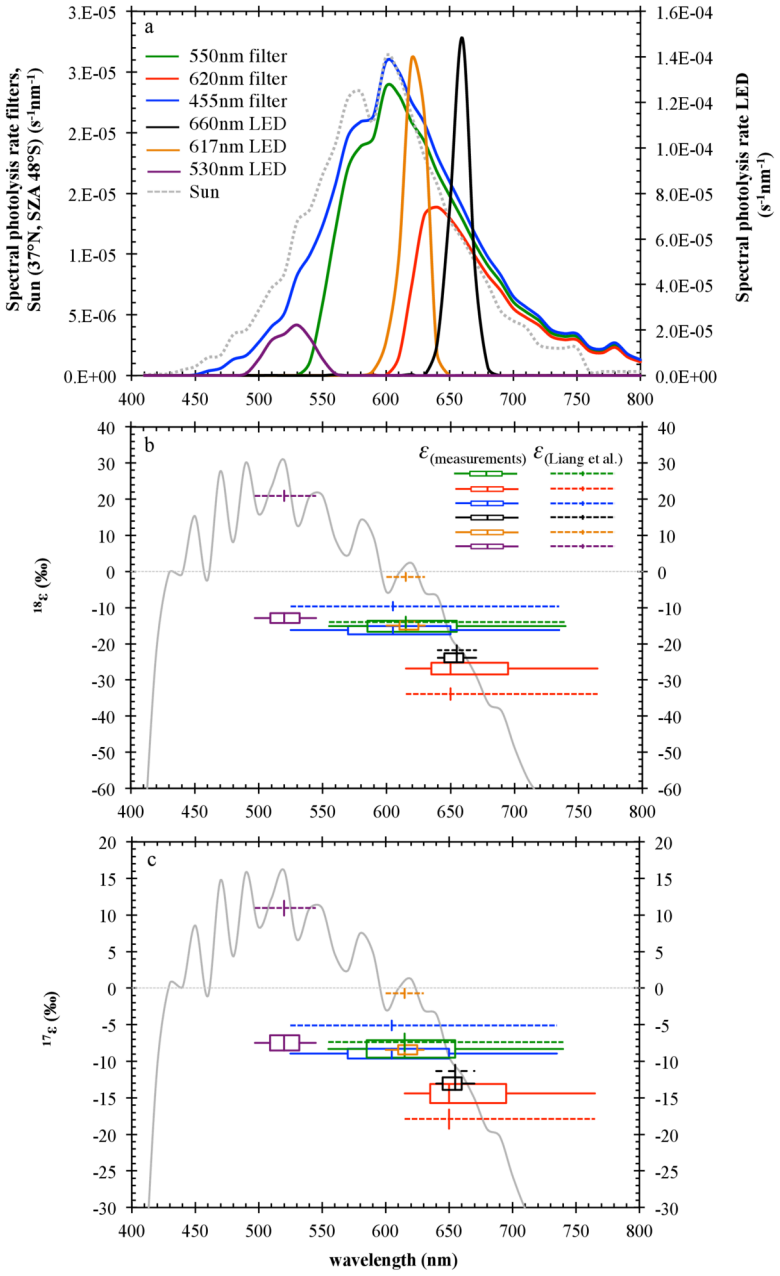

2015gl064192_figure02

©2015 American Geophysical Union. All rights reserved.

Accepted Article

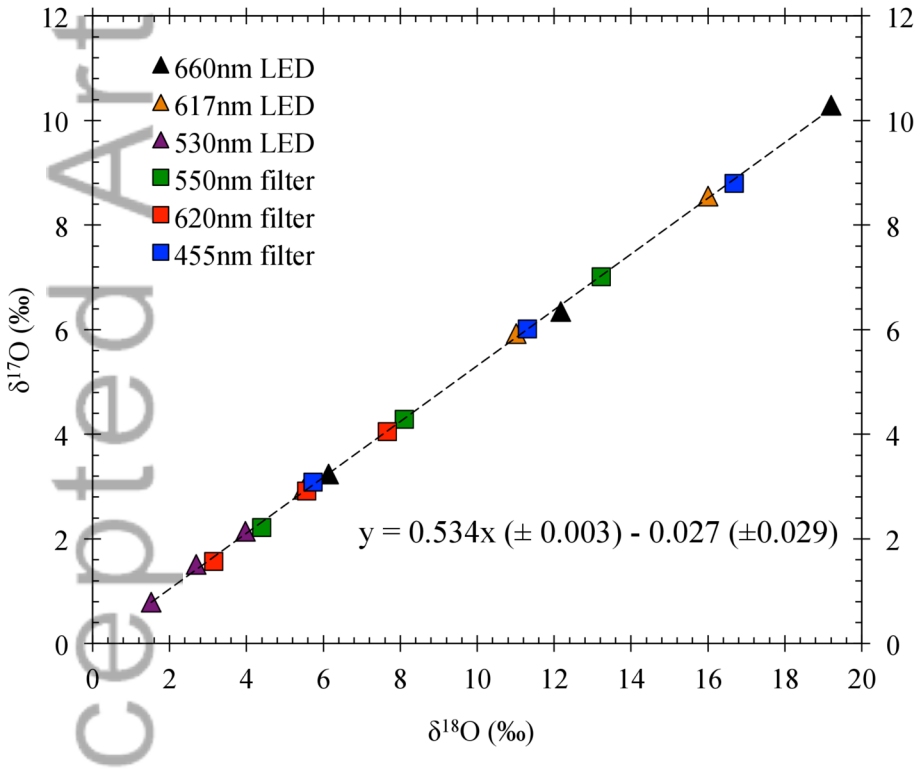

2015gl064192_figure03

©2015 American Geophysical Union. All rights reserved.

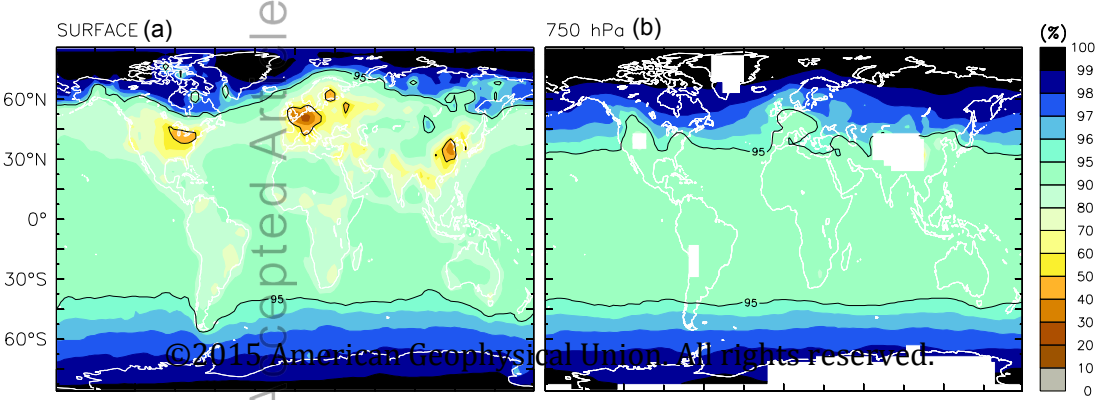

Accepted Article

©2015 American Geophysical Union. All rights reserved.